Environmental Science & Technology

pubs.acs.org/est

Article

Sunlight Photolysis of Extracellular and Intracellular Antibiotic Resistance Genes *tetA* and *sul2* in Photosensitizer-Free Water

Fiona B. Dunn and Andrea I. Silverman*

Cite This: *Environ. Sci. Technol.* 2021, 55, 11019−11028

Read Online

ACCESS | Metrics & More | Article Recommendations | Supporting Information

ABSTRACT: Antibiotic resistance genes (ARGs; the genetic material in bacteria that encode for resistance to antibiotics) have been found in the aquatic environment, raising concerns of an environmental transmission route. In an effort to contribute to models predicting the fate of ARGs in the environment—to design control measures, predict health risks, inform ARG surveillance activities, and prioritize policy interventions—and given the importance of sunlight in damaging DNA, we evaluated the sunlight photolysis kinetics of antibiotic-resistant bacteria (ARB) and ARGs under laboratory conditions, focusing on *Escherichia coli* SMS-3-5 and its ARGs *tetA* and *sul2*. Experiments were conducted in the absence of photosensitizers, and ARG decay rates were quantified by quantitative polymerase chain reaction (qPCR) with short and long amplicon targets. Long amplicon qPCR targets quantified greater photolysis rate constants, due to greater ARG coverage. After a lag phase, intracellular ARG had faster decay rates than extracellular ARG, likely due to the contribution of intracellular indirect photolysis processes. Furthermore, all ARG decay rates were significantly slower than those of *E. coli*. Decay rate constants and quantum yields are presented as foundational work in the development of models to describe the persistence of ARGs in sunlit, environmental waters.

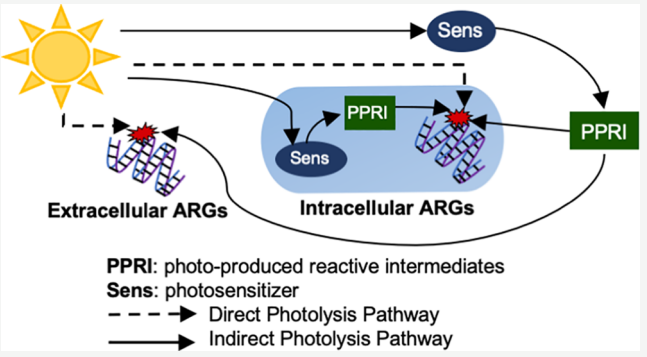

KEYWORDS: *DNA decay, direct photolysis, antibiotic-resistant bacteria, quantum yield, environmental persistence*

INTRODUCTION

Antibiotic-resistant bacteria (ARB) are a growing global health threat and jeopardize the ability of doctors to treat patients using commonly prescribed antibiotics. The United States Centers for Disease Control and Prevention estimate that in the United States alone, approximately 2.8 million people develop antibiotic-resistant infections each year, leading to 35 900 annual deaths.[1] In 2016, the United Nations declared antibiotic resistance to be the "greatest and most urgent global risk, requiring increased attention and coherence at the international, national, and regional levels".[2]

ARB are often excreted in the feces or urine of infected individuals, resulting in the presence of ARB and antibiotic resistance genes (ARGs, i.e., DNA that codes for antibiotic-resistant traits) in wastewater and at wastewater treatment facilities.[3,4] The presence of ARB and ARGs in wastewater can present a challenge for the design and operation of water and wastewater treatment processes: while ARB can be inactivated by commonly used disinfectants, ARGs may be resistant to decay,[5,6] and often persist through wastewater treatment processes and enter the environment.[7] Additionally, given that many regions of the world lack sanitation infrastructure and an estimated 80% of the world's wastewater is discharged without treatment,[8] ARB and ARGs are commonly discharged to the environment without prior disinfection. Waste streams from agricultural livestock operations have also been found to contain antibiotics and ARGs.[9,10] As a result, several studies have found ARGs in aqueous environments, including surface waters,[11] groundwater,[12] and river sediment.[13,14] Once in the environment, there is concern that ARGs may pose a public health risk, given that intra- and extracellular ARGs may convey resistance to surrounding bacteria through horizontal gene transfer mechanisms.[7]

In the natural water environment, and engineered treatment systems such as wastewater treatment ponds, sunlight is an important environmental stressor capable of microbial inactivation.[15] Sunlight exposure has been found to inactivate microorganisms,[16] including fecal indicator bacteria,[15,17] waterborne human viruses,[18,19] and bacteriophages.[18−20] Sunlight is also known to damage DNA through direct and indirect photolysis.[21] Direct photolysis occurs when a photon

Received: February 1, 2021
Revised: July 20, 2021
Accepted: July 21, 2021
Published: August 4, 2021

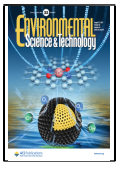

https://doi.org/10.1021/acs.est.1c00732
Environ. Sci. Technol. 2021, 55, 11019−11028

of light is absorbed by DNA, which leads to damages through the formation of photoproducts. The most commonly formed DNA photoproducts are cyclobutane pyrimidine dimers (CPD), in which adjacent pyrimidine bases (i.e., cytosine and thymine) dimerize;[22,23] additional photoproducts of direct photolysis include 6-4 photoproducts.[22,23] Alternatively, indirect photolysis involves photon absorption by intracellular or extracellular photosensitizers, which subsequently form highly damaging photochemically produced reactive intermediates (PPRI).[16] Singlet oxygen ($^1O_2$), an important PPRI in indirect photolysis of DNA, has been observed to damage guanine bases, forming photoproducts such as 8-oxo-7, 8-dihydro-2′-deoxyguanosine (8-oxodGuo).[24]

Given the frequent detection of ARGs in the aquatic environment and limited information available on their rates of decay in sunlit waters, the goal of this research was to evaluate and model the decay kinetics of ARB, and extracellular and intracellular ARGs due to sunlight photolysis in clear water (i.e., in the absence of exogenous photosensitizers). In particular, laboratory-based experiments using simulated sunlight were conducted to quantify direct photolysis rates and quantum yields of the ARGs *tetA* and *sul2*, which encode for resistance to tetracycline and sulfonamides, respectively, and inactivation kinetics of the antibiotic-resistant *Escherichia coli* strain SMS-3-5 that contains both ARGs on the same plasmid. The ARGs *tetA* and *sul2* have previously been found in the water environment. For example, an extensive study on the ARG load in the influent and effluent of European wastewater treatment plants detected *sul2* by quantitative PCR (qPCR) in over 90% of treated wastewater effluent samples analyzed.[3] Stoll et al. detected *sul2* by PCR in 77 and 100%, and *tetA* in 7 and 18% of surface water samples analyzed from Germany and Australia, respectively.[11] Li and Zhang detected *tetA* and *sul2* by qPCR in 100% of biofilm, sediment, and water samples analyzed from the Weihe River, China.[25]

Previous work has focused on the role of engineered disinfectants, including UV_{254}, on the decay kinetics and loss of function of chromosomal ARGs[6] and ARGs on small, high copy number plasmids—such as pUC19 [2686 base pairs (bp) in length][26,27] and pWH1266 (8890 bp)[28] with corresponding model bacterial transformation systems. In this work, we contribute to the literature on ARG photolysis with a focus on sunlight irradiance, which differs from UV_{254} and for which there is less data available in the literature. We also focus on a much larger plasmid (pSMS35_130; 130 440 bp), originating from the environmentally isolated *E. coli* SMS-3-5, which harbors several antibiotic resistance genes.

Given previous research that demonstrated that DNA photolysis rates may be underestimated when quantified using only a short section of a gene or genome,[28,29] sunlight damage to each ARG was quantified using two qPCR assays: one with a standard-length amplicon target and one with a longer amplicon target (LA-qPCR; 744-1054 bp). qPCR using a standard-length amplicon target [referred to as short amplicon qPCR (SA-qPCR) herein] is a common method used in surveillance studies of ARG in the environment.[30−33] However, SA-qPCR is typically conducted using an amplicon target that is less than 200 bp, which is a small subset of the total length of the genes of interest (i.e., on the order of 10^3 bp), and therefore may not fully detect DNA damage across the gene. Measured ARG photolysis rate constants were used to develop a modeling framework for sunlight photolysis of ARG and to quantify direct photolysis quantum yields.

MATERIALS AND METHODS

Antibiotic-Resistant Bacteria and Genes. *E. coli* SMS-3-5 (ATCC BAA-1743) was kindly provided by Dr. Amy Pruden's laboratory at Virginia Tech. Fricke et al. found that *E. coli* SMS-3-5 was tolerant of or resistant to 32 of 33 antibiotics tested, including resistance to tetracycline and sulfonamides (e.g., sulfathiazole, trimethoprim, and a trimethoprim−sulfamethoxazole mixture).[34] The *tetA* and *sul2* genes targeted in the present study reside on the same 130 440 base pair (bp) plasmid pSMS35_130 (GenBank: CP000971.1) within the genome of *E. coli* SMS-3-5. The *tetA* gene is 1275 bp long and covers region 120487-121761 on the plasmid; *sul2* is 816 bp long and covers region 97753-98568. The sequences of *tetA* and *sul2* are provided in the Supporting Information (SI).

Preparation of ARB and ARGs. *E. coli* SMS-3-5 were stored as glycerol stocks at −80 °C. To propagate bacteria, 100 μL of the glycerol stocks were inoculated into 25 mL of Luria−Bertani (LB) broth (10 g L^{-1} tryptone, 5 g L^{-1} yeast extract, 10 g L^{-1} NaCl) with 15 mg L^{-1} ampicillin and streptomycin antibiotics. After overnight incubation at 37 °C (on a rotary shaker at 50 rpm), the bacteria were inoculated into fresh broth and incubated overnight again at 37 °C. The bacterial culture was then washed four times through centrifugation at 10 000 rpm for 5 min and resuspension in 25 mL of sterile phosphate-buffered saline (PBS; 4.3 mM NaH_2PO_4, 15.8 mM Na_2HPO_4, 145.4 mM NaCl, pH 7.5). The washed bacteria were diluted to the final volume for experimentation and mixed in the dark for 10−18 h before use in intracellular photolysis experiments.

To obtain stock solutions of extracellular ARG, DNA was extracted from stationary phase *E. coli* SMS-3−5 cells using the DNeasy Blood & Tissue Kit (Qiagen). Extracted DNA was eluted in Buffer AE (provided by Qiagen: 10 mM Tris-Cl, 0.5 mM ethylenediaminetetraacetic acid (EDTA), pH 9), aliquoted, and frozen at −80 °C until use in experiments.

Simulated Sunlight Photolysis Experiments. Sunlight photolysis experiments were conducted for up to 72.5 h using a 1600 W solar simulator (Newport no. 94081A) with an ozone-free Xenon bulb (Newport no. 62726), an AM0 air mass filter (Newport no. 81311), and an atmospheric attenuation filter (Newport no. 71SI00091) to approximate a collimated beam of sunlight; the uniformity of the beam was within 5% across the irradiated area. The irradiance spectrum was measured at the start of each experiment using a Stellarnet BLK-C spectroradiometer (CR2 cosine receptor). The absorbance spectrum of each experimental solution was measured using a Cary Series UV−Vis−NIR spectrophotometer (Agilent Technologies). The solar simulator irradiance spectrum and experimental solution absorbance spectra are provided in the SI (Figure S1).

Separate experiments were conducted evaluating the photolysis of extracellular and intracellular ARGs. To evaluate simulated sunlight photolysis rates of extracellular ARG, extracted DNA was diluted 10× in sterile PBS; PBS was made in nuclease-free water, pasteurized, and filter-sterilized through a 0.2 μm nylon membrane before use. The initial total DNA concentration for the extracellular experiments was 2.68 ± 0.40 ng μL^{-1}, measured using the Qubit 1X dsDNA HS Assay kit (Thermo Fisher Scientific). Two hundred microliter volumes of the experimental solution were aliquoted into sterile 10 mm diameter polypropylene tubes (Biologix Group Limited no. 88-0103); the resulting solution depth was 0.5 cm.

https://doi.org/10.1021/acs.est.1c00732
Environ. Sci. Technol. 2021, 55, 11019−11028

The open tubes were placed underneath the solar simulator, in an aluminum cooling block in a water bath that was maintained at 18 ± 2 °C by a recirculating chiller. Sample tubes were covered with a 0.125 in. thick quartz plate (Technical Glass Products) to allow transmission of the full spectrum of simulated sunlight; the sides of the tubes were shaded by the cooling block, to ensure that light only entered from the top of the tubes, at an angle perpendicular to the surface of the solution. The bottom of the sample tubes had a slightly conical shape, but it was determined that the conical bottom did not have a significant influence on the calculation of photon flux. Dark control tubes were maintained in the same way, except covered with aluminum foil to block light exposure. Samples were collected sacrificially over time, by removing one tube for each sample point. To obtain better data resolution, some sample times were consistent across experiments, while others differed. Samples were immediately capped and stored at −80 °C until analyzed by qPCR.

To evaluate photolysis of intracellular ARG, experiments were conducted with ARB suspended in PBS with an average initial ARB concentration of $(6.07 \pm 4.86) \times 10^7$ colony forming units (CFU) mL^{-1}. One hundred and fifty milliliter volumes of the bacterial stock solution were aliquoted into 250 mL beakers that were painted black and mixed with magnetic stir bars. The resulting solution depth was 4.5 cm. Quartz discs were placed over the experimental reactors. Dark control reactors were covered in aluminum foil. The temperature was controlled using the water bath as described previously. One milliliter and 100 μL of subsamples were collected from each experimental reactor at set time points for DNA extraction and bacteria enumeration, respectively. Subsamples evaluated for concentrations of culturable bacteria were placed on ice in the dark and analyzed within 4 h. Subsamples evaluated for ARG decay were immediately stored at −80 °C until DNA extraction.

Enumeration of ARB. *E. coli* SMS-3-5 were enumerated as CFU using the spread plate method, with 20 μL inocula and LB agar (10 g L^{-1} tryptone, 1 g L^{-1} yeast extract, 8 g L^{-1} NaCl, 15 g L^{-1} agar). ARB inactivation rates were modeled using eq 1, in which C_0 is the initial bacteria concentration (CFU mL^{-1}), C_t is the concentration (CFU mL^{-1}) at time t (h), and $k_{obs,ARB}$ (h^{-1}) is the first-order observed inactivation rate constant of the ARB. To determine $k_{obs,ARB}$, replicate $-\ln\left(\frac{C_t}{C_0}\right)$ values for each time point were pooled and plotted versus time; $k_{obs,ARB}$ was calculated as the slope of the best-fit linear regression line. The standard error of $k_{obs,ARB}$ was calculated as the standard error of the slope.

$$\ln\left(\frac{C_t}{C_0}\right) = -k_{obs,ARB}t \quad (1)$$

Enumeration of ARGs by qPCR. Two qPCR assays were used to quantify each ARG. Long amplicon assays (LA-qPCR) targeted 1054 and 744 bp regions of the *tetA* and *sul2* genes, respectively, whereas short amplicon assays (SA-qPCR)[3] targeted 71 and 105 bp of *tetA* and *sul2*, respectively. Primer sequences are provided in Table S1. The primers for the *sul2* long amplicon assay were designed for this study using UGene software.[35] All other primer sequences were published previously.[3,5] All qPCR assays were conducted using a QuantStudio 3 real-time PCR system (Applied Biosystems), using SsoFast EvaGreen Supermix with Low ROX (Bio-Rad). Each 20 μL of qPCR reaction consisted of 10 μL of 2X Supermix, 400 nM of forward and reverse primers, 1 μL of template DNA, and sterile DNase-free water for dilution to the total volume.

The cycling parameters were the following: one cycle at 98 °C for 2 min, 40 cycles of 98 °C for 5 s, the annealing temperature (listed in Table S1 for each assay) for 10 s, and 72 °C for 65 s, followed by a melt curve. The elongation time of 65 s was used based on preliminary findings and results from the literature that showed an increase in qPCR efficiency with a longer elongation time for LA-qPCR.[36] All samples were analyzed in triplicate qPCR reactions. Serial dilutions of extracted DNA were run on each plate to quantify amplification efficiency. All efficiencies fell between 75 and 100% with the exception of two plates: R^2 values of the standard curves were consistently high [$R^2 = (0.97 \pm 0.03)$]. Given that whole extracted DNA was used to create standard curves for relative quantification, we believe that measured amplification efficiencies were good representations of the amplification efficiencies of individual samples.

Calculation of First-Order Decay Rate Constants for Extracellular ARG ($k^i_{obs,eARG}$). In this study, ARG decay was defined as the loss in qPCR signal over time. Relative ARG quantities were measured and used to calculate the first-order decay rate constant for each ARG, using a derived $\Delta\Delta Cq$ approach that is based on measured qPCR quantification cycle thresholds (Cq) for each sample, and the efficiency of the qPCR reaction. A derivation of the $\Delta\Delta Cq$ approach is detailed in the Supporting Information (eqs S5−S12), and its use in quantifying the first-order decay rate constant for extracellular ARG i ($k^i_{obs,eARG}$) is illustrated in eq 2, where Amp_F is the amplification factor of the qPCR reaction (equal to the decimal value of the amplification efficiency + 1; eq S10), Cq_0 is the qPCR quantification cycle for samples collected at $t = 0$, and Cq_t is the quantification cycle for samples collected at time t. To determine $k^i_{obs,eARG}$, replicate $\ln(Amp_F^{Cq0-Cqt})$ values for each time point were pooled and plotted versus time; $k^i_{obs,eARG}$ was calculated as the slope of the best-fit linear regression line.

$$\ln(Amp_F^{Cq_0-Cq_t}) = -k^i_{obs,eARG}t \quad (2)$$

Calculation of First-Order Decay Rate Constants for Intracellular ARG ($k^i_{obs,iARG}$). To quantify *tetA* and *sul2* decay in subsamples collected during intracellular photolysis experiments, DNA extraction was conducted for all samples from the same experiment at the same time. The total concentration of extracted DNA in each sample was determined using the Qubit 1X dsDNA HS Assay kit (Thermo Fischer Scientific). To account for potential differences in extraction efficiency between subsamples in the same time series (which could artificially impact observed DNA decay rates), and under the assumption that all subsamples should have the same total DNA concentration (given that they originated from the same stock solution), $\ln(Amp_F^{Cq0-Cqt})$ values for each sample were normalized by the measured extracted DNA concentrations (Figure S2). The resulting equation that describes the first-order observed decay rate constants for intracellular ARG i ($k^i_{obs,iARG}$) is presented as eq 3, where Y_0 is the total DNA concentration (ng μL^{-1}) of the extracted time $t = 0$ sample and Y_t is the total DNA concentration (ng μL^{-1}) of the extracted time t sample. The derivation of eq 3 is presented in the Supporting Information (eqs S13−S15). To determine $k^i_{obs,iARG}$, replicate $-\left(\ln(Amp_F^{Cq_0-Cq_t}) + \ln\left(\frac{Y_0}{Y_t}\right)\right)$ values for

https://doi.org/10.1021/acs.est.1c00732
Environ. Sci. Technol. 2021, 55, 11019−11028

each time point were pooled and plotted versus time; $k^i_{\text{obs,iARG}}$ were calculated as the slope of the best-fit linear regression line.

$$\ln(\text{Amp}_{\text{F}}{}^{Cq_0 - Cq_t}) + \ln\left(\frac{Y_0}{Y_t}\right) = -k^i_{\text{obs,iARG}}t \tag{3}$$

In addition to the log-linear first-order decay model described in eq 3, a multitarget model was used to calculate the first-order decay rate constant for intracellular ARG ($k^i_{\text{obs,iARG},m}$), to account for shoulders observed in the intracellular ARG decay curves. This method has been previously described in detail by Silverman et al.[37] The equation for the multitarget model is provided in eq 4, where m^i is the shoulder constant.

$$\ln(\text{Amp}_{\text{F}}{}^{Cq_0 - Cq_t}) + \ln\left(\frac{Y_0}{Y_t}\right) = \ln(1 - (1 - \exp(-k^i_{\text{obs,iARG,m}}t))^{m^i}) \tag{4}$$

Quantum Yield of Direct Photolysis. In the context of this study, the quantum yield of direct photolysis (ϕ^i) is the ratio of mol ARG i degraded (as quantified by LA-qPCR) to mol photons absorbed by the long amplicon target of the ARG. ϕ^i of direct photolysis (eq 5) were calculated based on measured decay rates from extracellular DNA decay experiments ($k^i_{\text{obs,eARG}}$), given that it is assumed that only direct photolysis was involved in DNA damage during these experiments, whereas there was potential of additional processes (e.g., endogenous indirect photolysis and DNA repair) to occur during intracellular photolysis experiments. The decay rate of the long amplicon qPCR target was used as a proxy for the decay rate of the full gene. This assumption was based on similar lengths of the long amplicon target and the gene. For example, the long amplicon target for *tetA* covers 82.7% of the gene, and that of *sul2* covers 91.2% of the gene (a summary of amplicon lengths is provided in Table S1).

$$\phi^i = k^i_{\text{obs,eARG}}\left(2.303 \sum_{280\text{ nm}}^{350\text{ nm}} \langle p^0_\lambda \rangle \cdot \varepsilon_{\lambda,\text{normDNA}} \cdot \varepsilon^i_{265} \cdot \Delta\lambda\right)^{-1} \tag{5}$$

In eq 5, $\varepsilon_{\lambda,\text{normDNA}}$ is a DNA photoaction spectrum that consists of values normalized by the value at 265 nm (unitless), ε^i_{265} is the extinction coefficient of the double-stranded, long amplicon qPCR target of ARG i at 265 nm [L(mol ARG)$^{-1}$ cm^{-1}], $\langle p^0_\lambda \rangle$ is the spectrum of average photon flux density transmitted through the water column (mol photons m^{-2} s^{-1} nm^{-1}), which was calculated based on the solar simulator irradiance spectrum (described in eqs S1−S3 of the Supporting Information), and $\Delta\lambda$ is the wavelength interval (nm) between measurements for each spectrum ($\Delta\lambda$ = 1 nm herein). The summation in eq 5 was calculated over a range of wavelengths from 280 to 350 nm; negligible photons are absorbed by the DNA at wavelengths greater than 350 nm (Figure 1b). The 2.303 conversion factor in eq 5 was used to convert the decadic absorbance spectra (used in the determination of the ε^i_{265} by Tataurov et al.[38]) to Napierian.

$\varepsilon_{\lambda,\text{normDNA}}$ describes the wavelength-dependent relative sensitivity of DNA to light and was determined by extracting photoaction spectrum data presented in a figure by Setlow et al.[39] using WebPlotDigitizer,[40] then fitting a curve through the data using a four-parameter logistics curve using GraphPad Prism 8 software (eq 6). We chose to use the DNA photoaction spectrum instead of extinction coefficient spectra

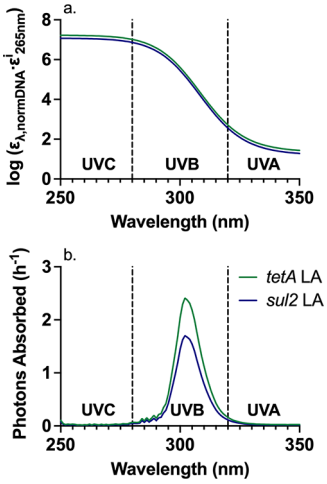

Figure 1. (a) Adjusted photoaction spectra [i.e., $\log(\varepsilon_{\lambda,\text{normDNA}} \cdot \varepsilon^i_{265})$; (L mol^{-1} cm^{-1})] for double-stranded, long amplicon (LA) qPCR targets of *tetA* and *sul2*, and (b) action-weighted photon absorbance spectra, i.e., $\langle p^0_\lambda \rangle \cdot \varepsilon_{\lambda,\text{normDNA}} \cdot \varepsilon^i_{265}$ of the double-stranded, long amplicon targets of *tetA* and *sul2*. The interfaces of UVC (100−280 nm), UVB (280−320 nm), and UVA (320−400 nm) regions are shown as vertical lines. The percentage of total photons absorbed for both the *tetA* and *sul2* long amplicon targets are 94 and 4% in the UVB and UVA regions, respectively.

in eq 5 given that we were unable to determine wavelength-specific values of ϕ^i due to the broadband nature of the solar simulator. Previous research has illustrated wavelength-specific sensitivity for the quantum yield of formation of CPD,[23] and we therefore assume that there is wavelength specificity to ϕ^i. The use of the DNA photoaction spectrum, which bundles both the wavelength-specific light absorbance of DNA and wavelength-specific sensitivity to damage into one spectrum, allows us to account for differences in ϕ^i across the incident light spectrum. Therefore, in essence, the ϕ^i determined herein are scaling factors for this sensitivity curve.

$$\log(\varepsilon_{\lambda,\text{normDNA}}) = -5.84 + \frac{5.88 \cdot \lambda^{-33.5}}{\lambda^{-33.5} + 308.8^{-33.5}} \tag{6}$$

$\varepsilon_{\lambda,\text{normDNA}}$ consists of a spectrum of values normalized by the value at 265 nm (i.e., $\varepsilon_{265,\text{normDNA}}$ = 1). To obtain absolute values, ε^i_{265} (the extinction coefficient of ARG i at 265 nm) was used to adjust the magnitude of $\varepsilon_{\lambda,\text{normDNA}}$ for specific DNA targets. ε^i_{265} was determined to be 1.54 × 10^7 and 1.09 × 10^7 L mol^{-1} cm^{-1} for the double-stranded, long amplicon sequences of *tetA* and *sul2*, respectively, using the nearest-neighbor model by Tataurov et al.,[38] which estimates nucleic acid extinction coefficients based on the DNA sequence and interactions between adjacent bases and base pairs. The DNA photoaction spectra [i.e., $\log(\varepsilon_{\lambda,\text{normDNA}} \cdot \varepsilon^i_{265})$] and action-weighted photon absorption spectra (i.e., $\langle p^0_\lambda \rangle \cdot \varepsilon_{\lambda,\text{normDNA}} \cdot \varepsilon^i_{265} \cdot \Delta\lambda$) for each long amplicon ARG target are presented in Figure 1.

Statistical Analysis. All statistical analyses were conducted in GraphPad Prism 8 software. Two-tailed hypothesis tests were conducted to test the null hypothesis that slopes of best-fit linear regressions are the same and therefore determine if first-order reaction rate constants were significantly different from each other. *P*-values were computed at a 95% confidence interval, where *P* less than 0.05 indicates significant differences. All rate constants are presented with the standard error, unless stated otherwise.

https://doi.org/10.1021/acs.est.1c00732
Environ. Sci. Technol. 2021, 55, 11019−11028

RESULTS AND DISCUSSION

Extracellular ARG Photolysis. The first-order observed photolysis rate constants of extracellular ARG in PBS ($k^i_{obs,eARG}$), measured using LA-qPCR, were (2.22 ± 0.14) × 10^{-2} h^{-1} (R^2 = 0.90) and (1.57 ± 0.17) × 10^{-2} h^{-1} (R^2 = 0.73) for *tetA* and *sul2*, respectively (Figure 2); $k^i_{obs,eARG}$ of the two

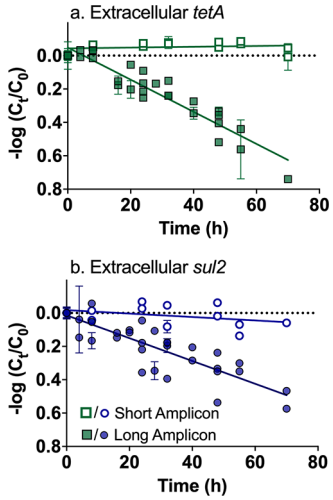

Figure 2. Simulated sunlight photolysis of extracellular ARG (a) *tetA* and (b) *sul*2 in PBS. Each point represents individual replicate measurements from four experiments conducted on two separate days. Error bars represent the standard deviation of triplicate qPCR reactions for that data point.

extracellular ARG were found to be significantly different from each other (P < 0.01). These $k^i_{obs,eARG}$ resulted in approximately 0.76 log and 0.52 log decay of extracellular *tetA* and *sul2* over 70 h, respectively. Given that experiments were conducted in photosensitizer-free solution, ARG degradation was attributed to the direct photolysis mechanism. Furthermore, $k^i_{obs,eARG}$ in dark control samples quantified using LA-qPCR were found to be insignificant (Figure S3): the dark decay rate of *sul2* [(−1.81 ± 1.30) × 10^{-3} h^{-1} (R^2 = 0.12)] was not statistically different from zero (P = 0.18); the dark decay rate of *tetA* [(6.05 ± 2.74) × 10^{-3} h^{-1} (R^2 = 0.27)] was similarly low; however, it was found to differ statistically from zero (P < 0.05). These results indicate that dark processes did not contribute to ARG decay in this experimental system, and all decay can be attributed to photolysis.

Extracellular ARG decay rate constants measured using SA-qPCR were significantly lower than those measured with LA-qPCR (P < 0.0001; Figure 2). The SA-qPCR decay rate constant of *sul2* was low [(2.54 ± 1.05) × 10^{-3} h^{-1} (R^2 = 0.22)], although statistically different from zero (P < 0.05); the decay rate constant for *tetA* [(−1.21 ± 1.02) × 10^{-3} h^{-1} (R^2 = 0.06)] was not found to be significantly different from zero (P = 0.25). For the *tetA* SA-qPCR assay, some qPCR reactions (at a seemingly random frequency) produced a melt curve that exhibited two peaks, indicating the possible formation of an additional nontarget PCR product. We reanalyzed the data after removing data points that had a second peak in the melt curve and found no impact on the measured *tetA* SA-qPCR $k^i_{obs,eARG}$. Nonetheless, if this assay were to be used in the future, one should be aware of the potential issue.

Our SA-qPCR findings parallel others in the literature. For example, studies evaluating UV_{254} decay of ARG have observed decay rate constants to increase with the length of the qPCR amplicon, which was attributed to an increase in the number of UV_{254} damage targets being captured by the assay.[6,26−28,41] Chang et al. evaluated UV_{254} inactivation of extracellular ARGs on a plasmid pWH1266 (containing *tetA* and bla_{TEM-1}) and quantified ARG decay using SA-qPCR, LA-qPCR, and transformation assays.[28] Chang et al. observed that first-order decay rate constants of ARGs quantified using LA-qPCR were larger than those using SA-qPCR, and also found that LA-qPCR underestimated loss of ARG transformation.[28] He et al., in their study on UV_{254} inactivation of the chromosomal ARG *blt* from *Bacillus subtilis* 1A189,[6] and Nihemaiti et al., in their study on UV_{254} inactivation of amp^R encoded in plasmid pUC19,[27] had similar findings: ARG degradation quantified by qPCR using amplicons of 266 bp and less than 400 bp, respectively, underestimated ARG deactivation (as quantified using transformation assays). Additionally, Nihemaiti et al. showed that the deactivation kinetics of amp^R was also dependent on the recipient cell used in transformation experiments, and the cell's ability to repair DNA.[27] Additional research is needed to understand if similar phenomena apply here in regard to loss of gene function due to sunlight photolysis.

While an ongoing objective of this work is to quantify the loss of gene function due to sunlight photolysis, we were unable to assess a decay in function of *tetA* and *sul2* on the plasmid evaluated herein due to its size (130 440 bp), and the challenges of conducting bacterial transformation with large plasmids. We attempted to conduct transformation using One Shot MAX Efficiency DH10B-T1^R Competent Cells (Invitrogen; Catalog no. 12331-013; assay conducted according to the manufacturer's instructions) and through electroporation using MegaX DH10B-T1^R Electrocompetent Cells [Invitrogen; Catalog no. C640003; assay conducted according to the manufacturer's instructions using Bio-Rad Micro Bio-Spin P-6 Gel columns with Tris buffer to desalt DNA samples, and a Bio-Rad MicroPulser to electroporate samples using a preprogrammed setting for *E. coli* (V = 2.5 kV)]. For both assays, the transformation control (i.e., the supercoiled pUC19 plasmid with an ampicillin resistance gene) was able to confer ampicillin resistance to recipient cells, indicating that the assay itself was working; however, DNA extracted from *E. coli* SMS-3-5 was not able to confer tetracycline or sulfamethoxazole resistance to recipient cells. The inability to transform recipient bacteria with the plasmid used in our experiments could be due to an inability of the recipient cells to uptake large plasmids or due to shearing of the plasmid during the DNA extraction from the *E. coli* SMS-3-5 cells, which could displace genetic elements necessary for gene expression (e.g., promoter regions). Although other studies have demonstrated the quantification of ARGs using smaller plasmids and model transformation systems,[27−29] additional method development and optimization is required to assess loss of gene function of ARGs originating from large, low copy number, environmentally isolated plasmids. Nonetheless, we hypothesize that direct sunlight photolysis will result in a faster decay of ARG function than the decay of the LA-qPCR signal.

Given that measured decay rates depend on qPCR amplicon length (in effect, the number of potential sites of CPD formation), $k^i_{obs,eARG}$ were normalized by the length of the LA-qPCR assays to enable comparison between targets; this normalized value was designated k^i_{norm} (h^{-1} bp^{-1}) (eq S16). The resulting $k^i_{norm,eARG}$ of extracellular *tetA* and *sul2* were not

https://doi.org/10.1021/acs.est.1c00732
Environ. Sci. Technol. 2021, 55, 11019−11028

significantly different from each other; the average $k^i_{norm,eARG}$ ± standard deviation was (2.11 ± 0.18) × 10^{-5} h^{-1} bp^{-1}. An additional analysis was conducted to calculate the decay rate constants as a function of the number of potential CPD sites in each qPCR amplicon (Table S3): extracellular decay rate constants determined using LA-qPCR were normalized by the number of adjacent thymine sites (TT; eq S17) in the double-stranded sequence of the long amplicon assays (Table S4). The average $k^i_{norm,eARG,TT}$ ± standard deviation was (2.56 ± 0.25) × 10^{-4} (h^{-1}(TT doublets)$^{-1}$). We did not model decay rate constants based on all potential CDP sites (i.e., TT, TC, CT, CC) due to limited knowledge on the wavelength specificity of the relative quantum yields of formation and molar absorptivities of each CPD. Nonetheless, modeling based on the number of TT is valuable given that TT sites have greater photoreactivity than the other CPDs.[42]

Zhang et al.[29] previously studied the photolysis of extracellular ARGs *tetA* and bla_{TEM-1} on the pBR322 plasmid (4361 bp), with exposure to 290−400 nm light in PBS. To compare our results, we used the decay rate constants quantified using LA-qPCR and the length of the LA-qPCR assay targets reported by Zhang et al. to calculate an average $k^i_{norm,eARG}$ from their experiments conducted in PBS, which we found to be (3.86 ± 0.62) × 10^{-4} h^{-1} bp^{-1}. We hypothesize that $k^i_{norm,eARG}$ from Zhang et al.[29] is greater than our calculated value due to potential differences in irradiance spectra or experimental setup between studies. For example, the irradiance spectrum from the light source used by Zhang et al.[29] was not provided in the manuscript; therefore, the proportion of light with shorter, more highly damaging UVB wavelengths is unknown. Additionally, the light source used by Zhang et al.[29] was a merry-go-round photochemical reactor that used quartz test tubes to hold the experimental solution. Nguyen et al.,[43] and references cited therein, previously documented that the geometry of quartz test tubes affects inactivation kinetics. Sunlight photolysis rates have been found to be greater when measured in quartz tubes than those measured in open beakers due to the fact that light can enter quartz tubes from all sides and be reflected internally off the walls of the tubes.[43]

Qiao et al.[44] conducted a literature review of decay rates of naked double-stranded DNA (dsDNA) with exposure to UV_{254}, which included data previously published by Chang et al.[28] and Yoon et al.[41] Recent studies have provided additional data on the UV_{254} decay kinetics of extracellular ARGs.[6,26,27] Using reported decay rate constants (quantified using qPCR amplicons that cover at least 70% of the total ARG length) and the reported lengths of the qPCR amplicons utilized, we calculated the average UV_{254} decay rate constants per bp of DNA, presented with the standard deviation, from several studies: (3.19 ± 1.08) × 10^{-5} cm^2 mJ^{-1} bp^{-1}, (7.43 ± 1.56) × 10^{-5} cm^2 mJ^{-1} bp^{-1}, (1.04 ± 0.20) × 10^{-4} cm^2 mJ^{-1} bp^{-1}, (8.81 ± 0.22) × 10^{-5} cm^2 mJ^{-1} bp^{-1}, and (1.00 ± 0.06) × 10^{-4} cm^2 mJ^{-1} bp^{-1} from Chang et al.,[28] Yoon et al.,[41] Yoon et al.,[26] He et al.,[6] and Nihemaiti et al.,[27] respectively. Using the sum of irradiance in the UVB region (i.e., 280−320 nm), we converted our average extracellular ARG decay rate constant to be in terms of fluence: (2.22 ± 0.19) × 10^{-8} cm^2 mJ^{-1} bp^{-1}. As expected, due to the sensitivity of DNA to UV_{254} irradiation and the absence of UV_{254} in simulated sunlight, the decay rate constants determined by the cited studies were several orders of magnitude greater than our observed decay rate constants for extracellular ARGs with exposure to simulated sunlight.

Intracellular ARG Photolysis and ARB Inactivation. Sunlight inactivation of the bacterium *E. coli* SMS-3-5 followed first-order kinetics, with an inactivation rate of (7.93 ± 1.00) × 10^{-1} h^{-1} (R^2 = 0.55) (Figure 3a). Intracellular *tetA* and *sul2* decay rate constants in dark control samples quantified using LA-qPCR were not significantly different from zero (P = 0.06 and 0.37 respectively, Figure S3). Due to the challenges with the *tetA* short amplicon assay mentioned above, SA-qPCR was conducted only on *sul2*, which resulted in $k^i_{obs,iARG}$ of simulated sunlight-exposed *sul2* to be equal to (9.14 ± 3.19) × 10^{-3} h^{-1} (R^2 = 0.37), which was found to be statistically different from zero (P < 0.05).

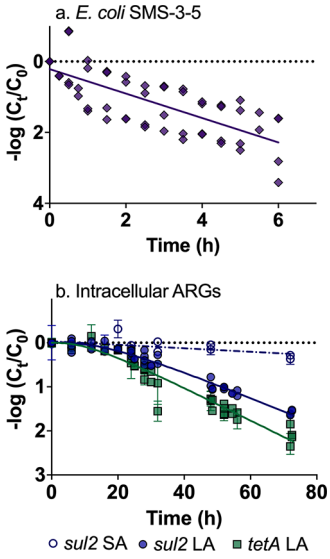

Figure 3. Simulated sunlight photolysis of (a) the bacterium *E. coli* SMS-3-5 and (b) intracellular ARGs in PBS. In panel (a), each marker represents individual replicate measurements from four experiments conducted on two separate days, and the solid line represents the best-fit linear regression line for the ARB. In panel (b), each marker represents individual replicate measurements from six experiments conducted on three separate days, error bars represent the standard deviation of triplicate qPCR reactions for that data point, and solid lines represent the best-fit lines of the multitarget model (eq 4) for each ARG long amplicon (LA) target. The dashed line represents the best-fit linear regression line for the short amplicon (SA) target of *sul2*. Please note that the scales of the *x*- and *y*-axes of panels (a) and (b) differ.

Similar to the extracellular experiments, data from LA-qPCR assays resulted in greater decay rate constants for intracellular ARG photolysis than the SA-qPCR assays; the resulting $k^i_{obs,iARG}$, calculated using the log-linear model (eq 3), were (7.27 ± 0.32) × 10^{-2} h^{-1} (R^2 = 0.93) and (5.30 ± 0.20) × 10^{-2} h^{-1} (R^2 = 0.94) for *tetA* and *sul2*, respectively (Figure S3). These $k^i_{obs,iARG}$ were significantly lower than that of the bacterium, which is consistent with observations from studies evaluating UV_{254} decay of ARGs.[5,28,41] When normalized by the length of the amplicon (eq S16), $k^i_{norm,iARG}$ of intracellular *tetA* and *sul2* were not significantly different from each other (P = 0.58), and the average was (7.01 ± 0.29) × 10^{-5} h^{-1} bp^{-1}. Given the insignificant loss of the SA-qPCR signal over time during experiments, we believe that the decay in LA-qPCR signal was not the result of plasmid loss by the bacteria during experiments. Additionally, the use of DNA extraction methodology that involves pelleting bacteria before extracting DNA

https://doi.org/10.1021/acs.est.1c00732
Environ. Sci. Technol. 2021, 55, 11019−11028

from the pellet (which would exclude extracellular DNA in the supernatant) allows us to attribute measured ARG decay to intracellular photolysis.

A lag in photolysis was observed in LA-qPCR intracellular ARG decay curves (Figure 3b), indicating that minimal photolysis was observed in the first ∼16 h of the experiments. Therefore, a multitarget kinetic model (eq 4) was also used to estimate the first-order photolysis rate constants of intracellular ARG ($k^i_{obs,eARG,m}$), presented with the standard error of the linear region (postshoulder) of the model; $k^i_{obs,eARG,m}$ were $(8.58 \pm 0.39) \times 10^{-2}$ h^{-1} (m = 2.97, R^2 = 0.94) and $(6.96 \pm 0.21) \times 10^{-2}$ h^{-1} (m = 3.66, R^2 = 0.97) for *tetA* and *sul2*, respectively (Figure 3b). Over the course of the 72.5 h experiment, there were approximately 2.1 log and 1.5 log decay of intracellular *tetA* and *sul2*, respectively. The use of the multitarget model improved the fit for intracellular ARG photolysis data, in comparison to the log-linear model.

Given that a lag phase before ARG decay was observed for intracellular ARG and not extracellular ARG, we hypothesize that factors related to being within bacterial cells result in an initial resistance of intracellular ARG to photolysis. One such mechanism is the ability of bacteria to repair sunlight-damaged DNA,[45,46] through direct reversal, nucleotide excision repair, interstrand crosslink repair, translesion synthesis, or homologous recombination.[47] Nihemaiti et al., for example, attributed a lower than expected rate of UV_{254} deactivation of the ampicillin resistance gene amp^R encoded in plasmid pUC19 (quantified as a reduction of gene function as determined through transformation assays) to DNA repair by transformed cells.[27] In the present work, after an initial lag period, log-linear ARG decay was observed, potentially due to accumulated DNA damage that outpaced rates of repair or inactivation of bacteria cells that resulted in inactivation of DNA repair mechanisms. Given that the lag in ARG decay lasted ∼16 h despite substantial *E. coli* inactivation observed in the first few hours of the experiment (Figure 3a), an open question is whether the bacterial enzymes involved in DNA repair continued to function even after the bacteria were no longer culturable.

Another difference in the photolysis kinetics between intracellular and extracellular ARG was the observed magnitudes of their decay rate constants. To compare the rate constants, given that the intracellular and extracellular ARG experimental solutions had different light absorbance spectra, $k^i_{obs,iARG}$ and $k^i_{obs,eARG}$ were first normalized by the average photon fluence transmitted through each solution (calculated for wavelengths between 280 and 400 nm; eqs S18−S22 in the SI); the resulting inactivation rates are designated as $k^i_{obs,iARG,photon}$ and $k^i_{obs,eARG,photon}$ [m^2 (mol photon)$^{-1}$]. To contextualize these rate constants, the endogenous sunlight inactivation rate of the single-stranded RNA bacteriophage MS2 was estimated using a previously published model that depends on sunlight irradiance, a wavelength-specific photon absorption rate, and the quantum yield of MS2 inactivation (described in the SI; eq S23).[48,49] A summary of all experimental and predicted $k^i_{obs,x,photon}$ values of ARGs, ARB, and relevant microorganisms are presented in Figure 4.

The photolysis rate constants of intracellular *tetA* and *sul2* ($k^i_{obs,iARG,photon}$) were found to be greater than those of extracellular ARG ($k^i_{obs,eARG,photon}$) and the predicted value for MS2. In a recent review, it was hypothesized that extracellular ARG decay could be faster than intracellular decay, partially due to DNA repair mechanisms in bacterial cells.[16] We observed that this hypothesis was true in our sensitizer-free matrices for only the first 16 h of the experiment, after which the photolysis rates of intracellular *tetA* and *sul2* were significantly greater than that of the extracellular ARGs. We hypothesize that this was due to a contribution of indirect photolysis within cells, resulting from the formation of intracellular PPRI by intracellular photosensitizers. In our clear-water experimental system, in the absence of extracellular photosensitizers, we assume that extracellular ARG decay was due to direct photolysis alone and therefore slower. It is possible that the relative magnitude of intracellular and extracellular photolysis could be different in environmental waters containing PPRI-producing photosensitizers.

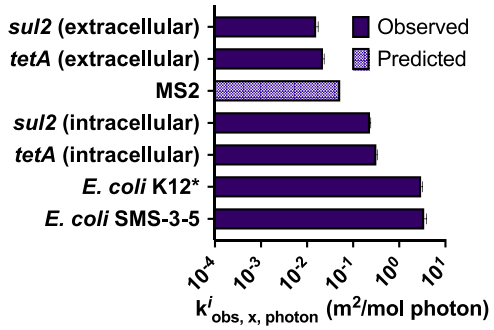

Figure 4. Comparison of photolysis rates that were normalized by the average photon fluence (280−400 nm) transmitted through the solution ($k^i_{obs,x,photon}$). Error bars on observed values indicate standard error. The 95% confidence intervals were not available for the calculation of the predicted $k^i_{obs,x,photon}$ for MS2. *E. coli* K12 data were provided by Chiyenge and Silverman.[50]

When converted to be in terms of photon fluence, we found that the observed solar inactivation rate constant of the bacterium *E. coli* SMS-3-5 was very similar to that of laboratory-cultured *E. coli* K12 [ATCC 10798; quantified by Chiyenge and Silverman (manuscript to be submitted for publication) under similar experimental conditions: in PBS at pH 7 with exposure to full-spectrum sunlight from the same solar simulator (Figure S4)].[50] *E. coli* K12 is a commonly used model organism with a different antibiotic-resistance profile than *E. coli* SMS-3-5.[51] Al-Jassim et al. previously found *E. coli* PI-7—a wastewater-sourced, virulent, antibiotic-resistant strain—to be more resistant to simulated sunlight than *E. coli* DSM1103 (ATCC 25922), a strain that displayed lower virulence and reduced antibiotic resistance.[52] The increased resistance to irradiation observed for *E. coli* PI-7 was hypothesized to result from the upregulation of a collection of genes that regulate oxidative stress response mechanisms (such as efflux pumps and the production of reactive oxygen species scavengers) and cellular repair mechanisms (such as DNA repair and cell wall synthesis), which presents the possibility of mechanisms of cross resistance to antibiotics and photomediated damage.[52] Conversely, in the present study, we did not observe any difference in sensitivity to sunlight between the two strains of laboratory-cultured *E. coli* with different antibiotic-resistance profiles. Similarly, Giannakis et al.[53] studied the inactivation of ARB under solar and solar-photo-Fenton treatment and did not observe any notable difference in inactivation between antibiotic-resistant and antibiotic-susceptible strains.

https://doi.org/10.1021/acs.est.1c00732
Environ. Sci. Technol. 2021, 55, 11019−11028

Quantum Yield of Direct Photolysis. ϕ^i were calculated to be 2.72×10^{-6} and 2.73×10^{-6} for the double-stranded, long amplicon targets of *tetA* and *sul2*, respectively. The average quantum yield per bp was calculated as $(3.13 \pm 0.77) \times 10^{-9}$ bp^{-1}. It is difficult to directly compare these quantum yields to those currently published in the literature due to variation in quantification methods; experimental conditions, such as the microorganism or DNA oligomers used for experimentation; temperature, ionic strength, and pH of the experimental solution; and the presence of UV_{254} wavelengths.[42,44,54]

As described in the Methods section, there is a wavelength specificity to ϕ^i that was not possible to quantify with our experimental design, given that the solar simulator emits light over a range of wavelengths. Therefore, we chose to pair ϕ^i with a photoaction spectrum instead of an extinction coefficient spectrum in our direct photolysis model (eq 5) to account for differences in sensitivity at different wavelengths. The decision to take this approach was supported by data from Cadet and Douki,[23] who reported the yields of CPD formation with an exposure to light from different regions of the light spectrum. Based on the data from Cadet and Douki, the relative yields of CPD formation for UVA (310 nm)/UVB (290 nm)/UVC (254 nm) light are $1:(1.7 \times 10^4):(1.5 \times 10^5)$.[23] The relative values of the photoaction spectrum derived from Setlow[39] and used herein are $1:(2.2 \times 10^4):(1.6 \times 10^5)$ for UVA (average over 320−350 nm)/UVB (average over 280−320 nm)/UVC (254 nm) light, which are similar to the values from Cadet and Douki. We acknowledge that CPDs are not the only products of direct photolysis, but feel that the approximate comparison is valid because CPDs tend to be produced at rates greater than the other photoproducts.[23]

Given that we did not evaluate photolysis with exposure to UVC light, ϕ^i of direct photolysis of ARGs calculated in this study are for sunlight photolysis and may not be valid at shorter wavelengths. For example, we used the first-order decay rate constant of the *tetA* gene reported by Chang et al. under UV_{254} exposure using LA-qPCR to calculate ϕ^i at 254 nm using our model [$k_{obs} = (58 \pm 6) \times 10^{-3}$ cm^2 mJ^{-1}; UV_{254} irradiance = (0.18 ± 0.01) mW cm^{-2}].[28] In our calculations, we assumed that all of the measured irradiance was at 254 nm, no light attenuation occurred, and the target-specific extinction coefficient (ε^i_{265}) values were the same as the *tetA* gene in our study. Equation 5 was amended so that the variables $\varepsilon_{\lambda,normDNA}$ and $\langle p^0_\lambda \rangle$ were specific to λ = 254 nm. The resulting ϕ^i at 254 nm was 5.99×10^{-7} bp^{-1}, which is greater than the sunlight ϕ^i determined herein.

Environmental Implications. LA-qPCR was more sensitive to detecting DNA photolysis than SA-qPCR. Across all ARG studied, k_{obs} measured using LA-qPCR assays were significantly greater from those measured using SA-qPCR assays, with the latter indicating less than 0.06 log decay of eARGs over the course of 70 h. Many environmental monitoring studies have utilized qPCR assays with relatively short amplicon targets (e.g., less than 200 bp) to quantify ARG in environmental matrices.[30−33] Given our findings, we suspect that these studies may overestimate the amount of undamaged ARG in sunlight-exposed environments and recommend that longer amplicon qPCR targets be used in future monitoring efforts to more accurately represent undamaged ARG concentrations. However, method development and optimization may be needed to overcome challenges in conducting LA-qPCR on samples from complex environmental matrices.

In this study, we defined ARG decay as a loss of qPCR signal and present an experimentally derived quantum yield of direct photolysis of ARGs that can be used to model the first-order decay rate constant of ARGs in sunlit systems. However, it is important to note that this does not necessarily represent the rate at which a loss of gene function occurs. As discussed above, additional methodological development is needed to assess the deactivation of ARGs located on large plasmids.

Sunlight photolysis of *E. coli* SMS-3-5 was significantly faster than that of both intracellular and extracellular *tetA* and *sul2* (Figure 4). Our results indicate that intracellular and extracellular ARGs may be much more persistent in the water environment than ARB and other health-relevant bacteria and viruses. However, as discussed previously, this work was conducted in sensitizer-free water matrices, without the contribution of extracellular indirect photolysis mechanisms that may increase ARG decay rates. Future research will evaluate sunlight photolysis of ARGs and ARB in more complex environmental matrices that may result in increased decay rates due to indirect photolysis and sunlight-independent inactivation processes.[29] Nonetheless, this work lays the important foundational groundwork in the development of models to describe the persistence of ARGs in sunlit, environmental waters.

■ ASSOCIATED CONTENT

Supporting Information

The Supporting Information is available free of charge at https://pubs.acs.org/doi/10.1021/acs.est.1c00732.

Additional methodology and supporting figures and tables including: solar simulator irradiance spectrum and absorbance spectra of experimental solutions; photon flux calculations; quantum yield calculations; qPCR assay parameters; derivation of ΔΔCq method and photolysis rate equation of extracellular ARG; DNA extraction normalization and photolysis rate equation of Intracellular ARG; decay rate constants normalized by qPCR amplicon length; ARG sequences; potential CPD site analysis and normalization based on number of TT doublets; calculation of first-order decay rate constants as a function of photon fluence; predicted endogenous sunlight inactivation rate of bacteriophage MS2; dark control data of the sunlight photolysis of ARGs in PBS; and solar inactivation data of *E. coli* K12 (PDF)

■ AUTHOR INFORMATION

Corresponding Author

Andrea I. Silverman − *Department of Civil and Urban Engineering, Tandon School of Engineering, New York University, Brooklyn, New York 11201, United States; School of Global Public Health, New York University, New York, New York 10003, United States;* orcid.org/0000-0001-8199-5860; Phone: 646-997-3018; Email: andrea.silverman@nyu.edu

Author

Fiona B. Dunn − *Department of Civil and Urban Engineering, Tandon School of Engineering, New York University, Brooklyn, New York 11201, United States*

Complete contact information is available at: https://pubs.acs.org/10.1021/acs.est.1c00732

Notes

The authors declare no competing financial interest.

■ ACKNOWLEDGMENTS

This work was supported by the United States National Science Foundation (NSF CBET-1846692). F.B.D. is supported by an NSF Graduate Research Fellowship. The authors thank Dr. Amy Pruden and Dr. Dongjuan Dai for providing *E. coli* SMS-3-5, Chinedu Odibeli and Savannah Sookchan for assistance in the laboratory, Dr. Elizabeth Hénaff for assistance in designing long amplicon primers, and Mwale Chiyenge for sharing data.

■ REFERENCES

(1) Centers for Disease Control and Prevention (U.S.). Antibiotic Resistance Threats in the United States, 2019. 2019, https://doi.org/10.15620/cdc:82532.

(2) Mushtaq, A. UN Commits to Tackling Antimicrobial Resistance. *Lancet Infect. Dis.* **2016**, *16*, 1229−1230.

(3) Pärnänen, K. M. M.; Narciso-da-Rocha, C.; Kneis, D.; Berendonk, T. U.; Cacace, D.; Do, T. T.; Elpers, C.; Fatta-Kassinos, D.; Henriques, I.; Jaeger, T.; Karkman, A.; Martinez, J. L.; Michael, S. G.; Michael-Kordatou, I.; O'Sullivan, K.; Rodriguez-Mozaz, S.; Schwartz, T.; Sheng, H.; Sørum, H.; Stedtfeld, R. D.; Tiedje, J. M.; Giustina, S. V. D.; Walsh, F.; Vaz-Moreira, I.; Virta, M.; Manaia, C. M. Antibiotic Resistance in European Wastewater Treatment Plants Mirrors the Pattern of Clinical Antibiotic Resistance Prevalence. *Sci. Adv.* **2019**, *5*, No. eaau9124.

(4) Auerbach, E. A.; Seyfried, E. E.; McMahon, K. D. Tetracycline Resistance Genes in Activated Sludge Wastewater Treatment Plants. *Water Res.* **2007**, *41*, 1143−1151.

(5) McKinney, C. W.; Pruden, A. Ultraviolet Disinfection of Antibiotic Resistant Bacteria and Their Antibiotic Resistance Genes in Water and Wastewater. *Environ. Sci. Technol.* **2012**, *46*, 13393−13400.

(6) He, H.; Zhou, P.; Shimabuku, K. K.; Fang, X.; Li, S.; Lee, Y.; Dodd, M. C. Degradation and Deactivation of Bacterial Antibiotic Resistance Genes during Exposure to Free Chlorine, Monochloramine, Chlorine Dioxide, Ozone, Ultraviolet Light, and Hydroxyl Radical. *Environ. Sci. Technol.* **2019**, *53*, 2013−2026.

(7) Dodd, M. C. Potential Impacts of Disinfection Processes on Elimination and Deactivation of Antibiotic Resistance Genes during Water and Wastewater Treatment. *J. Environ. Monit.* **2012**, *14*, 1754−1771.

(8) UNESCO, UN-Water. *United Nations World Water Development Report 2020: Water and Climate Change; Paris*, 2020.

(9) He, Y.; Yuan, Q.; Mathieu, J.; Stadler, L.; Senehi, N.; Sun, R.; Alvarez, P. J. J. Antibiotic Resistance Genes from Livestock Waste: Occurrence, Dissemination, and Treatment. *npj Clean Water* **2020**, *3*, 1−11.

(10) Peak, N.; Knapp, C. W.; Yang, R. K.; Hanfelt, M. M.; Smith, M. S.; Aga, D. S.; Graham, D. W. Abundance of Six Tetracycline Resistance Genes in Wastewater Lagoons at Cattle Feedlots with Different Antibiotic Use Strategies. *Environ. Microbiol.* **2007**, *9*, 143−151.

(11) Stoll, C.; Sidhu, J. P. S.; Tiehm, A.; Toze, S. Prevalence of Clinically Relevant Antibiotic Resistance Genes in Surface Water Samples Collected from Germany and Australia. *Environ. Sci. Technol.* **2012**, *46*, 9716−9726.

(12) Koike, S.; Krapac, I. G.; Oliver, H. D.; Yannarell, A. C.; Chee-Sanford, J. C.; Aminov, R. I.; Mackie, R. I. Monitoring and Source Tracking of Tetracycline Resistance Genes in Lagoons and Groundwater Adjacent to Swine Production Facilities over a 3-Year Period. *Appl. Environ. Microbiol.* **2007**, *73*, 4813−4823.

(13) Pruden, A.; Arabi, M.; Storteboom, H. N. Correlation Between Upstream Human Activities and Riverine Antibiotic Resistance Genes. *Environ. Sci. Technol.* **2012**, *46*, 11541−11549.

(14) Pruden, A.; Pei, R.; Storteboom, H.; Carlson, K. H. Antibiotic Resistance Genes as Emerging Contaminants: Studies in Northern Colorado. *Environ. Sci. Technol.* **2006**, *40*, 7445−7450.

(15) Davies-Colley, R. J.; Donnison, A. M.; Speed, D. J.; Ross, C. M.; Nagels, J. W. Inactivation of Faecal Indicator Micro-Organisms in Waste Stabilisation Ponds: Interactions of Environmental Factors with Sunlight. *Water Res.* **1999**, *33*, 1220−1230.

(16) Nelson, K. L.; Boehm, A. B.; Davies-Colley, R. J.; Dodd, M. C.; Kohn, T.; Linden, K. G.; Liu, Y.; Maraccini, P. A.; McNeill, K.; Mitch, W. A.; Nguyen, T. H.; Parker, K. M.; Rodriguez, R. A.; Sassoubre, L. M.; Silverman, A. I.; Wigginton, K. R.; Zepp, R. G. Sunlight-Mediated Inactivation of Health-Relevant Microorganisms in Water: A Review of Mechanisms and Modeling Approaches. *Environ. Sci.: Processes Impacts* **2018**, *20*, 1089−1122.

(17) Sassoubre, L. M.; Nelson, K. L.; Boehm, A. B. Mechanisms for Photoinactivation of Enterococcus Faecalis in Seawater. *Appl. Environ. Microbiol.* **2012**, *78*, 7776−7785.

(18) Silverman, A. I.; Peterson, B. M.; Boehm, A. B.; McNeill, K.; Nelson, K. L. Sunlight Inactivation of Human Viruses and Bacteriophages in Coastal Waters Containing Natural Photosensitizers. *Environ. Sci. Technol.* **2013**, *47*, 1870−1878.

(19) Silverman, A. I.; Nguyen, M. T.; Schilling, I. E.; Wenk, J.; Nelson, K. L. Sunlight Inactivation of Viruses in Open-Water Unit Process Treatment Wetlands: Modeling Endogenous and Exogenous Inactivation Rates. *Environ. Sci. Technol.* **2015**, *49*, 2757−2766.

(20) Kohn, T.; Nelson, K. L. Sunlight-Mediated Inactivation of MS2 Coliphage via Exogenous Singlet Oxygen Produced by Sensitizers in Natural Waters. *Environ. Sci. Technol.* **2007**, *41*, 192−197.

(21) Jagger, J. *Solar-UV Actions on Living Cells*; Praeger: New York, 1985.

(22) Görner, H. New Trends in Photobiology: Photochemistry of DNA and Related Biomolecules: Quantum Yields and Consequences of Photoionization. *J. Photochem. Photobiol., B* **1994**, *26*, 117−139.

(23) Cadet, J.; Douki, T. Formation of UV-Induced DNA Damage Contributing to Skin Cancer Development. *Photochem. Photobiol. Sci.* **2018**, *17*, 1816−1841.

(24) Ravanat, J.-L.; Douki, T.; Cadet, J. Direct and Indirect Effects of UV Radiation on DNA and Its Components. *J. Photochem. Photobiol., B* **2001**, *63*, 88−102.

(25) Li, Q.; Zhang, Q. Prevalence and Pollution Characteristics of Antibiotic Resistant Genes in One High Anthropogenically-Impacted River. *PLoS One* **2020**, *15*, No. e0231128.

(26) Yoon, Y.; Dodd, M. C.; Lee, Y. Elimination of Transforming Activity and Gene Degradation during UV and UV/H2O2 Treatment of Plasmid-Encoded Antibiotic Resistance Genes. *Environ. Sci.: Water Res. Technol.* **2018**, *4*, 1239−1251.

(27) Nihemaiti, M.; Yoon, Y.; He, H.; Dodd, M. C.; Croué, J.-P.; Lee, Y. Degradation and Deactivation of a Plasmid-Encoded Extracellular Antibiotic Resistance Gene during Separate and Combined Exposures to UV254 and Radicals. *Water Res.* **2020**, *182*, No. 115921.

(28) Chang, P. H.; Juhrend, B.; Olson, T. M.; Marrs, C. F.; Wigginton, K. R. Degradation of Extracellular Antibiotic Resistance Genes with UV254 Treatment. *Environ. Sci. Technol.* **2017**, *51*, 6185−6192.

(29) Zhang, X.; Li, J.; Fan, W.-Y.; Yao, M.-C.; Yuan, L.; Sheng, G.-P. Enhanced Photodegradation of Extracellular Antibiotic Resistance Genes by Dissolved Organic Matter Photosensitization. *Environ. Sci. Technol.* **2019**, *53*, 10732−10740.

(30) Wang, X.; Gu, J.; Gao, H.; Qian, X.; Li, H. Abundances of Clinically Relevant Antibiotic Resistance Genes and Bacterial Community Diversity in the Weihe River, China. *Int. J. Environ. Res. Public Health* **2018**, *15*, No. 708.

(31) Xiong, W.; Sun, Y.; Zhang, T.; Ding, X.; Li, Y.; Wang, M.; Zeng, Z. Antibiotics, Antibiotic Resistance Genes, and Bacterial Community Composition in Fresh Water Aquaculture Environment in China. *Microb. Ecol.* **2015**, *70*, 425−432.

(32) Wang, M.; Liu, P.; Xiong, W.; Zhou, Q.; Wangxiao, J.; Zeng, Z.; Sun, Y. Fate of Potential Indicator Antimicrobial Resistance Genes

(ARGs) and Bacterial Community Diversity in Simulated Manure-Soil Microcosms. *Ecotoxicol. Environ. Saf.* **2018**, *147*, 817−823.
(33) Rodriguez-Mozaz, S.; Chamorro, S.; Marti, E.; Huerta, B.; Gros, M.; Sànchez-Melsió, A.; Borrego, C. M.; Barceló, D.; Balcázar, J. L. Occurrence of Antibiotics and Antibiotic Resistance Genes in Hospital and Urban Wastewaters and Their Impact on the Receiving River. *Water Res.* **2015**, *69*, 234−242.
(34) Fricke, W. F.; Wright, M. S.; Lindell, A. H.; Harkins, D. M.; Baker-Austin, C.; Ravel, J.; Stepanauskas, R. Insights into the Environmental Resistance Gene Pool from the Genome Sequence of the Multidrug-Resistant Environmental Isolate Escherichia Coli SMS-3-5. *J. Bacteriol.* **2008**, *190*, 6779−6794.
(35) Okonechnikov, K.; Golosova, O.; Fursov, M.; UGENE team. Unipro UGENE: A Unified Bioinformatics Toolkit. *Bioinformatics* **2012**, *28*, 1166−1167.
(36) Ho, J.; Seidel, M.; Niessner, R.; Eggers, J.; Tiehm, A. Long Amplicon (LA)-QPCR for the Discrimination of Infectious and Noninfectious Phix174 Bacteriophages after UV Inactivation. *Water Res.* **2016**, *103*, 141−148.
(37) Silverman, A. I.; Nelson, K. L. Modeling the Endogenous Sunlight Inactivation Rates of Laboratory Strain and Wastewater *E. coli* and Enterococci Using Biological Weighting Functions. *Environ. Sci. Technol.* **2016**, *50*, 12292−12301.
(38) Tataurov, A. V.; You, Y.; Owczarzy, R. Predicting Ultraviolet Spectrum of Single Stranded and Double Stranded Deoxyribonucleic Acids. *Biophys. Chem.* **2008**, *133*, 66−70.
(39) Setlow, R. B. The Wavelengths in Sunlight Effective in Producing Skin Cancer: A Theoretical Analysis. *Proc. Natl. Acad. Sci. U.S.A.* **1974**, *71*, 3363−3366.
(40) Rohatgi, A. WebPlotDigitizer; Pacifica, California, USA, 2020.
(41) Yoon, Y.; Chung, H. J.; Wen Di, D. Y.; Dodd, M. C.; Hur, H.-G.; Lee, Y. Inactivation Efficiency of Plasmid-Encoded Antibiotic Resistance Genes during Water Treatment with Chlorine, UV, and UV/H2O2. *Water Res.* **2017**, *123*, 783−793.
(42) Douki, T. Low Ionic Strength Reduces Cytosine Photoreactivity in UVC-Irradiated Isolated DNA. *Photochem. Photobiol. Sci.* **2006**, *5*, 1045−1051.
(43) Nguyen, M. T.; Silverman, A. I.; Nelson, K. L. Sunlight Inactivation of MS2 Coliphage in the Absence of Photosensitizers: Modeling the Endogenous Inactivation Rate Using a Photoaction Spectrum. *Environ. Sci. Technol.* **2014**, *48*, 3891−3898.
(44) Qiao, Z.; Ye, Y.; Chang, P. H.; Thirunarayanan, D.; Wigginton, K. R. Nucleic Acid Photolysis by UV254 and the Impact of Virus Encapsidation. *Environ. Sci. Technol.* **2018**, *52*, No. 10408.
(45) Häder, D.-P.; Sinha, R. P. Solar Ultraviolet Radiation-Induced DNA Damage in Aquatic Organisms: Potential Environmental Impact. *Mutat. Res., Fundam. Mol. Mech. Mutagen.* **2005**, *571*, 221−233.
(46) Sinha, R. P.; Häder, D.-P. UV-Induced DNA Damage and Repair: A Review. *Photochem. Photobiol. Sci.* **2002**, *1*, 225−236.
(47) Chatterjee, N.; Walker, G. C. Mechanisms of DNA Damage, Repair and Mutagenesis. *Environ. Mol. Mutagen.* **2017**, *58*, 235−263.
(48) Silverman, A. I.; Tay, N.; Machairas, N. Comparison of Biological Weighting Functions Used to Model Endogenous Sunlight Inactivation Rates of MS2 Coliphage. *Water Res.* **2019**, *151*, 439−446.
(49) Mattle, M. J.; Vione, D.; Kohn, T. Conceptual Model and Experimental Framework to Determine the Contributions of Direct and Indirect Photoreactions to the Solar Disinfection of MS2, PhiX174, and Adenovirus. *Environ. Sci. Technol.* **2015**, *49*, 334−342.
(50) Chiyenge, M.; Silverman, A. I. Effect of PH on the Rates of Endogenous Sunlight Inactivation of Laboratory Strain and Wastewater-Sourced *E. coli* and Enterococci, submitted for Publication.
(51) Du, J.; Singh, H.; Yi, T.-H. Biosynthesis of Silver Nanoparticles by Novosphingobium Sp. THG-C3 and Their Antimicrobial Potential. *Artif. Cells, Nanomed., Biotechnol.* **2017**, *45*, 211−217.
(52) Al-Jassim, N.; Mantilla-Calderon, D.; Wang, T.; Hong, P.-Y. Inactivation and Gene Expression of a Virulent Wastewater *Escherichia Coli* Strain and the Nonvirulent Commensal Escherichia Coli DSM1103 Strain upon Solar Irradiation. *Environ. Sci. Technol.* **2017**, *51*, 3649−3659.
(53) Giannakis, S.; Le, T.-T. M.; Entenza, J. M.; Pulgarin, C. Solar Photo-Fenton Disinfection of 11 Antibiotic-Resistant Bacteria (ARB) and Elimination of Representative AR Genes. Evidence That Antibiotic Resistance Does Not Imply Resistance to Oxidative Treatment. *Water Res.* **2018**, *143*, 334−345.
(54) Douki, T. Effect of Denaturation on the Photochemistry of Pyrimidine Bases in Isolated DNA. *J. Photochem. Photobiol., B* **2006**, *82*, 45−52.

NOTE ADDED AFTER ASAP PUBLICATION

This paper was published on August 4, 2021. Due to production error, it was paired with an incorrect synopsis. The corrected version was reposted on August 5, 2021.

https://doi.org/10.1021/acs.est.1c00732
Environ. Sci. Technol. 2021, 55, 11019−11028